RESEARCH ARTICLE

D. Saxena,* A. Fischer,*
J. Dranczewski, W. K. Ng, N. V. Trivino,
H. Schmid, T. V. Raziman,
A. Arnaudon, M. Barahona, O. Hess,
K. Moselund, R. Sapienza*...2400623

Designed Semiconductor Network Random Lasers

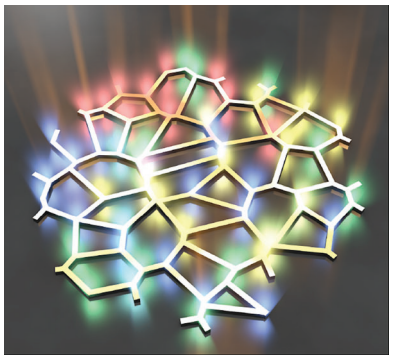

Complex networks designed and fabricated on a III-V semiconductor bonded layer show low-threshold multimode lasing that is highly sensitive to pump illumination and stable over intense optical pumping. The optimal design of the waveguides forming the network links and the density of nodes and links for efficient random lasing is investigated.

LASER & PHOTONICS REVIEWS
www.lpr-journal.org

Designed Semiconductor Network Random Lasers

Dhruv Saxena, Anna Fischer,* Jakub Dranczewski, Wai Kit Ng, Noelia Vico Trivino, Heinz Schmid, T. V. Raziman, Alexis Arnaudon, Mauricio Barahona, Ortwin Hess, Kirsten Moselund, and Riccardo Sapienza**

Conventional lasers typically support a well-defined comb of modes. Coupling many resonators together to form larger complex cavities enables the design of the spatial and spectral distribution of modes, for sensitive and controllable on-chip light sources. Network lasers, formed from a mesh of dye-doped polymer interconnecting waveguides, have shown great potential for random lasing with a highly sensitive and customizable lasing spectrum albeit suffering from gain bleaching. Here on-chip semiconductor network lasers are introduced, and fabricated by etching an InP epilayer bonded onto a SiO_2/Si wafer, as a reproducible, stable and designable random laser with a rich multimodal spectrum and low room temperature lasing threshold. Thresholds are observed as low as 60 μJcm^{-2} $pulse^{-1}$ for InP networks with an optimum link width of 450 nm and thickness of 120 nm. It is further shown, both experimentally and numerically, that the network density directly affects the mode spatial distribution, and lasing modes are spatially localized over only 10–20 connected links in large dense networks. The InP network lasers are also stable to pump illumination and sensitive to small variations in the pump pattern. These studies lay the ground for the future design of random lasers tailored to the application in robust semiconductor platforms with impact for sensing, signal processing, cryptography and machine learning.

1. Introduction

Lasers with tunable spectra are useful for many applications such as signal processing, on-chip optical communication,[1,2] and optical computing.[3–5] Multimode lasers enable applications that require low-coherence lasers to reduce artifacts such as speckle noise and crosstalk.[6] Complex laser cavities from coupled sub-units are emerging for applications as their properties can be tailored by both the geometry of individual units as well as their collective arrangement. Some examples include photonic crystal lasers,[7,8] hyperuniform lasers,[9] topological cavity lasers,[10,11] super-symmetric lasers[12] and random lasers.[13–17] Among these, random lasers, which are designed around diffusion and multiple scattering, are promising for their rich spatio-temporal modal dynamics, mode localization and spectral tunability by adaptive pumping.[18,19] Random lasers have been developed in various cavity configurations in 1D, 2D, and 3D, utilizing simple building blocks such as colloidal particles with a laser dye,[13] high-index semiconductor nanostructures[14] or inverse structures such as etched holes in the gain medium.[15–17] The 2D geometries offer the advantage of being planar and so the potential for integration with photonic chips and fabrication with semiconductor materials whereas 1D

D. Saxena, A. Fischer, J. Dranczewski, W. K. Ng, T. V. Raziman, O. Hess, R. Sapienza
Blackett Laboratory
Department of Physics
Imperial College London
London SW7 2AZ, UK
E-mail: d.saxena@imperial.ac.uk; anna.fischer@ibm.com; r.sapienza@imperial.ac.uk

A. Fischer, J. Dranczewski, N. V. Trivino, H. Schmid
IBM Research Europe - Zürich
Säumerstrasse 4
Rüschlikon 8803, Switzerland

The ORCID identification number(s) for the author(s) of this article can be found under https://doi.org/10.1002/lpor.202400623

DOI: 10.1002/lpor.202400623

T. V. Raziman, A. Arnaudon, M. Barahona
Department of Mathematics
Imperial College London
London SW7 2AZ, UK

A. Arnaudon
Blue Brain Project
École Polytechnique Fédérale de Lausanne (EPFL)
Campus Biotech
Geneva 1202, Switzerland

O. Hess
School of Physics and CRANN Institute
Trinity College Dublin
Dublin 2, Ireland

K. Moselund
Paul Scherrer Institut
Forschungsstrasse 111
Villigen 5232, Switzerland

K. Moselund
EPFL
Lausanne 1015, Switzerland

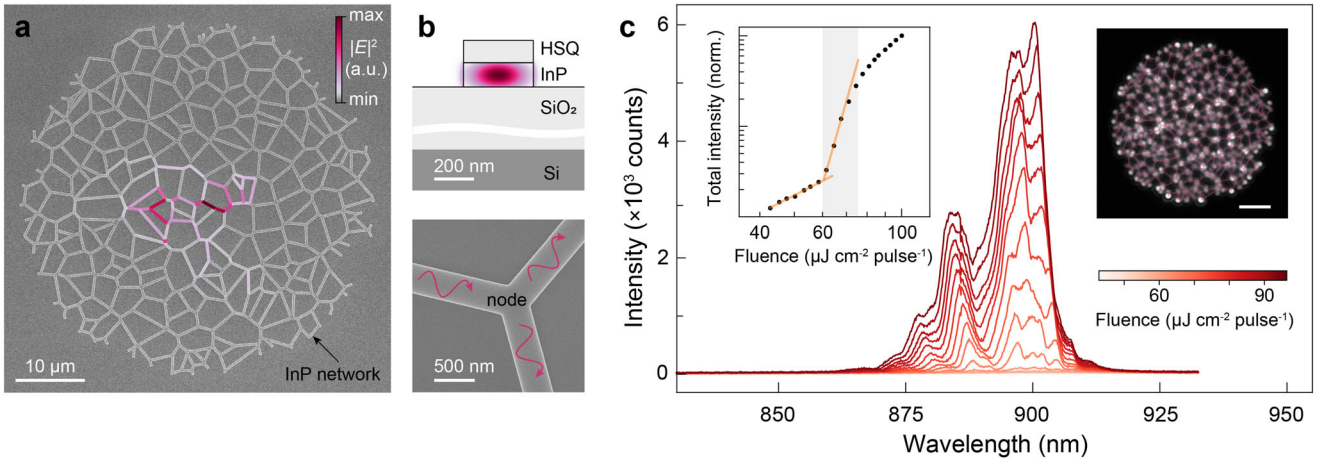

Figure 1. InP network laser. a) SEM image of a fabricated InP network with 50 μm diameter and 2 μm average link length on top of a SiO_2/Si substrate. b) Each link of the network guides light (top panel shows cross-section of one link with fundamental guided mode overlaid) and each node of the network scatters light into adjacent waveguides (bottom panel). Photonic modes in the network are formed by light interference across many closed paths. An example mode profile is superimposed over the network image in (a). c) Lasing is characterized by optical pumping at room temperature (lasing spectra in main panel and integrated intensity versus pump fluence in left inset). The device has a threshold fluence of 60 μJcm^{-2} pulse^{-1}. Optical image of the lasing from the network (right inset, scale bar 10 μm) shows strong emission localized at the network nodes.

geometries naturally offer the additional benefit of enhanced coupling due to the low dimensionality.

One emerging class of random lasers that combine the advantages of both 2D and 1D, are network lasers, which are quasi-1D, with a fractal dimension lower than 2, as they are made from an interconnected network of active waveguides embedded in 2D space.[20–23] The modes formed in the network arise from multiple scattering and interference across the network links and depend on the graph's physical structure and gain/loss profile.[24] The network can therefore be custom-designed and integrated on planar substrates, while offering strong confinement of light, efficient random lasing and directional output of light from network links. Network lasers have been made with self-assembled dye-doped polymer nanofibres,[23] but crucially lacking fabrication control and long life. Similarly, non-planar networks formed from a polymeric fibre mesh[25] and biological structures[26] have shown random lasing, however with limited control over their structure and connectivity. An alternative approach to using a disordered network as a random lasing medium has been to form a network of random lasers, by coupling different random lasers together on a plane[27] or with optical fibers,[28] but the number of coupled elements has been limited to a few.

Here we demonstrate intentionally designed, stable and robust random InP network lasers. We show efficient room temperature lasing with low thresholds around 60 μJcm^{-2} pulse^{-1} and wide-range, multimode emission centered around 900 nm. We study network lasers of different sizes and densities to gain insight into their effect on the lasing properties. We demonstrate that lasing occurs from network modes and characterize the mode spatial extent in networks by studying the lasing threshold under variable pump sizes. We additionally show that the waveguide thickness can be optimized to yield low thresholds. The good emission stability under prolonged pumping regimes and high spectral sensitivity to spatially changing pump lay the foundation for use in applications.

2. Results

Networks were fabricated on a thin InP membrane bonded to a SiO_2/Si substrate via a top-down method detailed in ref. [29] (see Experimental Section), which provides great network design flexibility and yields high-quality waveguides with smooth side walls and low propagation loss. InP is our material of choice because of its low surface recombination velocity and high optical quality.

The networks are region edges of Voronoi diagrams generated from a random point pattern, cropped into circular areas with diameters between 30–150 μm and average link lengths of 2–10 μm (**Figure 1a**; Table S1 and Figure S1, Supporting Information). The network links serve as waveguides for the light that is then scattered at the nodes (Figure 1b; Figure S2, Supporting Information). This leads to photonic network modes from constructive interference across many closed paths[23] (Figure S3, Supporting Information). One such mode profile is shown superimposed over the network SEM image in Figure 1a.

The InP network lasers show efficient room temperature lasing when optically pumped with a 700 nm, 200 fs-pulsed laser (see Experimental Section). The emission spectrum shows many resonant peaks between 870 and 920 nm corresponding to the InP gain region (Figure 1c; Figure S4, Supporting Information). The numerous peaks arise as the spatial disorder of the modes break symmetry and allows many modes with similar Q factor. The modes are broad compared to other lasing devices[23] due to band-filling and wavelength chirping effects common for bulk semiconductor lasers.[30–32] The far-field image of the network above the threshold (right inset Figure 1c; Figure S5, Supporting Information) shows bright emission from network nodes, due to strong waveguiding in the links and out-of-plane scattering of light at the nodes, as observed for previous network lasers.[23] Typical lasing characteristics, such as the "S" shape curve in the total light in versus total light out (LL) plot on the log–log scale are also observed (left inset Figure 1c; Figure S6, Supporting Information). The threshold fluence is obtained from the inter-

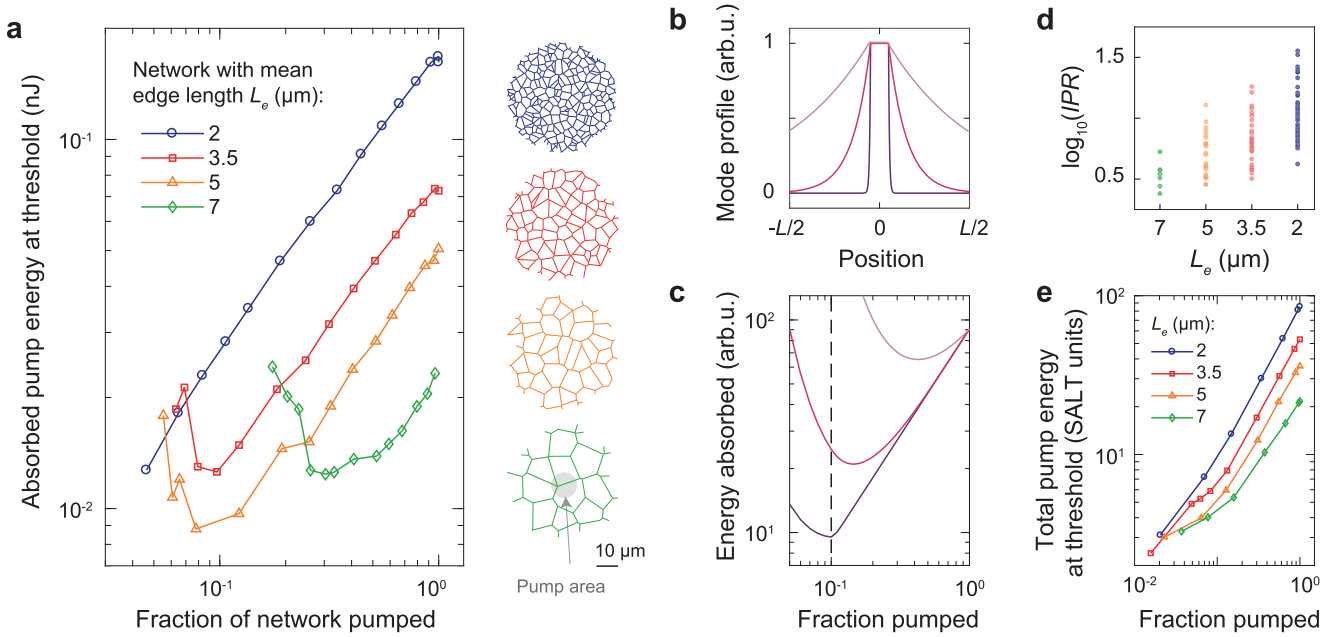

Figure 2. Threshold variation with pump size. a) Pump energy absorbed by the network at the lasing threshold versus fraction of the network pumped, for different Voronoi networks with 50 μm span and average edge lengths 2, 3.5, 5, and 7 μm respectively. Schematic of the different Voronoi networks is shown on the right. b,c) 1D model of the absorbed energy at threshold as function of the fraction pumped. The mode is centered within the cavity and has different spatial extents as shown in (b). In (c), considering logarithmic gain, the energy absorbed reduces linearly while the pump length is larger than the mode extent and then starts to increase sharply with further reduction in pump fraction. The position of the minimum in energy absorbed is dependent on the spatial extent. d,e) Model of the absorbed energy at threshold versus pump size using netSALT (with linear gain—see Note S3, Supporting Information). The inverse participation ratio (IPR) for the lasing modes of the different Voronoi networks when uniformly pumped is shown in (d). Large IPR indicates modes are spatially more localized. The pump energy at threshold in (e) is calculated by multiplying the first lasing threshold by the total length of the network pumped. The results in (e) agree qualitatively with experimental data in (a) for large pump fraction, where the threshold pump strength (proportional to threshold carrier density) is lowest and InP gain is approximately linear with pump strength.

section of two linear fits to the LL curve (shown by orange lines) and is as low as 60 μJcm^{-2} pulse^{-1}. This is comparable with values reported in the previous works with traditional whispering gallery geometry in InP.[33,34] From finite-difference time-domain (FDTD) simulations (see Experimental Section), we estimate a pump absorption cross-section of 4.8×10^{-6} cm^2 for this network, using which we get a threshold carrier density estimate of 1.5×10^{19} cm^{-3} (see Note S2, Supporting Information).

While there is clear evidence of lasing from networks, it is difficult to ascertain from the spectrum or far-field emission profile (Figure S7, Supporting Information) which modes are lasing and whether they are localized or delocalized, coupled or uncoupled. To investigate this, we examined the pump size dependence of lasing threshold, which is a useful technique for characterizing random lasers.[35,36] We varied the pump spot size on the networks and performed power sweeps to identify the lasing threshold at each pump size. A digital micromirror device (DMD) was used to control the pump spot size while maintaining a constant pump fluence on the sample (see Experimental Section). The absorbed energy at the threshold (calculated by multiplying the threshold fluence by the estimated absorption cross-section) versus the fraction of the network pumped (obtained from fluorescence images of the network pumped with different pump sizes—see Figure S8, Supporting Information) is presented in **Figure 2a**, for four different Voronoi networks of different node/link density (fixed span of 50 μm with average link lengths 2, 3.5, 5, and 7 μm). If the network was lasing from individual links serving as independent Fabry–Perot cavities, then the threshold energy would be unaffected by varying the pump size (see Note S3, Supporting Information). Instead, as we see in Figure 2a, the threshold energy is not independent of pump fraction: the threshold energy exhibits a monotonic decrease when the fraction of the network pumped is reduced. For the networks with medium and low density (average link lengths > 3 μm) the threshold energy reaches a minimum, which shifts to lower values of the pump fraction as the network density increases, after which the absorbed pump energy starts to increase with reduced pump fraction. Due to limited pump power available, a minimum in the threshold energy is not reached for the densest network (average link length 2 μm), and only the monotonic decrease with pump fraction reduction is seen.

To shed light on this variation of threshold energy with pump fraction for the different networks, we consider a 1D cavity that sustains lasing modes of various localization, as represented in Figure 2b. From steady state ab-initio laser theory (SALT), it is known that the threshold pump fluence (D_0) depends inversely on the pump overlap with the mode (see Note S3, Supporting Information). If the cavity is pumped at its center and the pump-size varied, the threshold variation with pump size will be qualitatively different between the two situations where the pump size is smaller or larger than the mode extent. With linear gain, the threshold energy (pump fluence times

total length pumped) varies linearly with pump fraction when the pump area is larger than the mode extent and is constant when the pump overlap is less than 1 (see Figure S9, Supporting Information). However, if the gain is logarithmic with pump fluence ($g = \log(D_0/D_{tr})$, where D_{tr} is the minimum pump fluence to achieve optical gain and $D_0 > D_{tr}$), which is more representative in semiconductors,[37] the threshold energy rises sharply for a reduction of the pump fraction (when the pump overlap is less than 1) because a much larger D_0 is needed to achieve the same threshold gain g_{th} compared to the linear case. Hence, the threshold energy versus pump fraction plot shows a minimum in threshold energy, whose position depends on the spatial extent of the lasing mode, as depicted in Figure 2c. This simple model which considers the spatial extent of the modes qualitatively describes the experimental observation of a linear decrease followed by a sharp increase of the pump energy of the lasing threshold under the reduction of pump area.

The spatial extent of modes in network lasers depends on the connectivity, size, and density,[23] and can be quantified by calculating the inverse participation ratio (IPR), where a larger IPR corresponds to a lower mode spread.[38] The IPR for lasing modes in each of the Voronoi networks, calculated using netSALT[24] (a theoretical model that combines graph theory with SALT – see Figure S3, Supporting Information), is presented in Figure 2d. The IPR distribution shifts to larger values as the average link length decreases (density increases). An intuitive explanation for this is that with increasing density, modes can be supported on smaller regions within the graph relative to its total area. The larger IPR, or smaller mode extent, for denser networks, correlates well with the experimental observation that the minima in threshold energy shifts to lower values of pump fraction, see Figure 2a. For 3.5 and 5 μm network lasers, the minima occurs at approximately 0.1 pump fraction (total length 770 and 520 μm, respectively), from which we deduce that the lasing modes extend over 10–20 connected links, consistent with the mode IPR shown in Figure 2d.

We further validate our model for pump-size dependence of threshold energy with netSALT calculations. Figure 2e presents the calculation of total pump strength at threshold versus the fraction of network pumped for each of the Voronoi networks. The total pump fluence at threshold is calculated by multiplying the threshold pump fluence of the first lasing mode by the length of the network pumped. Since the netSALT model uses linear gain, the results agree qualitatively with the experiments only at large pump fractions, where the threshold fluence is low and the gain in InP is approximately linear (Figure S10, Supporting Information).

Through this analysis we have shown, that the connectivity, size, and density of random lasers, which affect the mode extent, are an important design factor to tune the threshold behavior under different pump sizes.

Another important design consideration for a network laser, other than its topology, is the design of the waveguide links to obtain large mode confinement within the waveguide[39] and low-loss transmission of the guided modes through the network. Initial examination of mode loss in thick and thin waveguides using FDTD simulations indicated that wide, thin waveguides have lower scattering loss at nodes than narrow, thick waveguides (see Figures S11 and S12, Supporting Information). Thinner bonded layers also require less etch time and so would have less degradation from dry etching. Hence, the InP thickness in our networks was fixed at 120 nm.

With the thickness fixed, the waveguide width can be chosen to get low scattering loss at a node. For simplicity, we model a symmetric Y branch (degree 3 nodes with 120° angle between links) as depicted in **Figure 3a** with a cross-section as shown in Figure 1b and calculate the mode transmission using FDTD simulations (see Experimental Section). The set of guided modes supported in the waveguide depends on the waveguide width (Figure S13, Supporting Information). Unlike a suspended waveguide surrounded by air, the waveguides are multimode at all diameters (as seen in top panel Figure 3b) because the substrate introduces anisotropy in the waveguide geometry and lifts mode degeneracy.[40] As a consequence, the transmitted mode power from one link into adjoining links at the node is split into all available guided modes. We observe this in the field cross-section profiles in Figure 3a, where the field in adjoining links is not the same as that in the injected link.

In order to correctly assess the lasing threshold, we calculate the power transmitted from light traveling in a link into each supported guided mode in each link, essentially determining the full transmission matrix for the Y branch for a given waveguide width (see Figure S14, Supporting Information). The total power transmitted in a particular guided mode is thus a sum of the transmission matrix elements, including power transmitted into the same mode (for example TE01 mode to TE01 mode) and mode mixing terms (power coupled from a different injected mode, for example TM00 mode to TE01 mode). The total transmission versus waveguide width is shown in Figure 3b for the three lowest order modes. The highest transmission is for TE01 mode at a waveguide width of 450 nm, which also has the largest confinement factor. At larger waveguide widths, the total transmission into TE01 mode reduces due to coupling into higher order modes and at smaller waveguide widths, the total transmission reduces because of poor confinement from the cut-off (width of 350 nm). For waveguide widths below 350 nm, the transmitted power and confinement factor are the highest for the fundamental TE00 mode.

Low threshold lasing requires both a high transmission (low scattering loss) and high mode confinement (large modal gain.[41]) The calculations in Figure 3b predict the lowest lasing threshold at 450 nm waveguide width. We test this experimentally, by fabricating identical networks with three different waveguide widths (350, 450, and 550 nm). The networks were uniformly pumped and threshold measured from linear fits to the LL curves. Experimentally measured thresholds for several devices are shown in Figure 3c (see Note S1 and Figure S4, Supporting Information for threshold correction depending on pump wavelength). Consistent with the model predictions, the 450 nm-wide networks have the lowest thresholds (average of 60 $\mu J cm^{-2}$ $pulse^{-1}$) compared with the 350 nm and 550 nm-wide networks.

The InP network lasers are very stable toward degradation. We studied the lasing stability of a network with 150 μm diameter, 7 μm average link length, and 550 nm waveguide width under prolonged pumping. We pumped the network continuously with a 633 nm, 200 fs-pulsed laser at 100 kHz for 1.5 h, and acquired spectra every 5 s. The total emission intensity of these spectra only slightly (~20%) decreased over 4.5×10^8 pump pulses

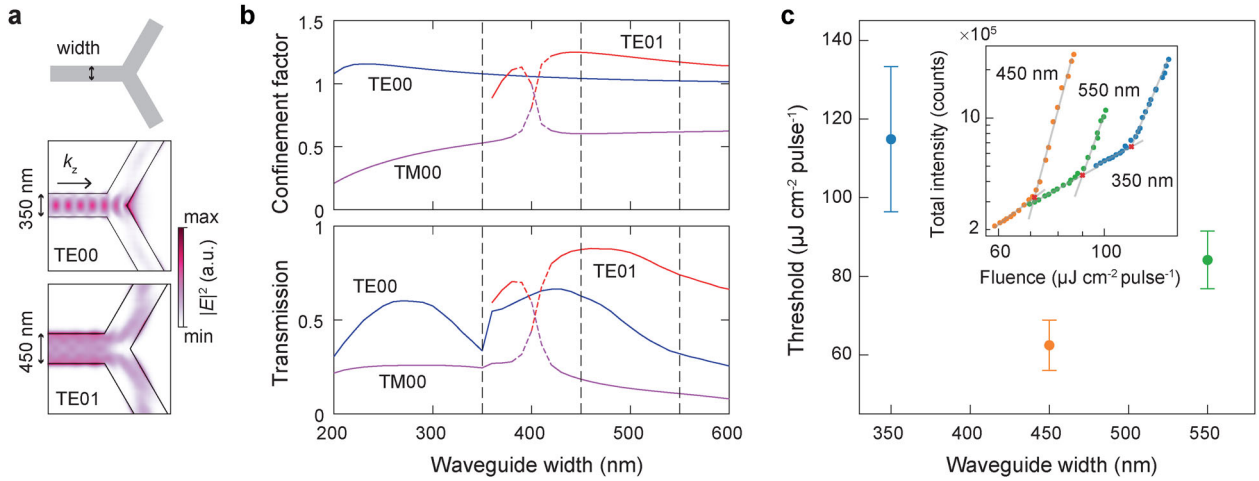

Figure 3. Threshold variation with waveguide width. a) The waveguide width in the network design is optimized to reduce lasing threshold, using FDTD simulations. Field profiles in the cross-section of a Y branch, for TE00 and TE01 mode in 350 and 450 nm wide waveguide, respectively. b) Above: Mode confinement factor[39] of the guided modes supported in network links as a function of waveguide width. Below: Total mode transmission in the Y branch for different waveguide widths, calculated from FDTD simulations (see Experimental Section). The total transmission includes both powers transmitted into the same mode (e.g., TE00 → TE00) and power converted into the mode from other modes (e.g., TE01 → TE00) (see Figure S14, Supporting Information). c) Experimentally determined thresholds for several Voronoi InP networks that are identical in graph topology but have different waveguide widths: 350, 450, and 550 nm. LL curve for three selected network lasers shown in inset.

(**Figure** 4a). Most importantly, the lasing threshold of the device only increased by 3% (from 42.6 to 43.9 μJ cm^{-2} pulse^{-1} after performing such an intense pumping regime, indicating no permanent damage (Figure 4b). Our InP network laser is much more stable than polymer-based ones.[23] The good stability of the device is further demonstrated by the similarity between the first and last acquired spectra (Figure 4c).

While the emission spectrum is highly stable over time, it is extremely sensitive toward spatial changes in the pump. Pumping the network with a spatially slightly different pump beam highly influences the emission spectrum. Figure 4d shows how the emission spectrum drastically changes when the network is pumped with different beam shapes: a homogeneous full disk (grey line), a disk with switched-off pixels forming a smiley face (purple line) and a disk with switched-off pixels forming a sad face (blue line). This sensitivity toward spatial changes in the pump has been theoretically predicted and can be used to tune the spectrum toward desired wavelengths.[24]

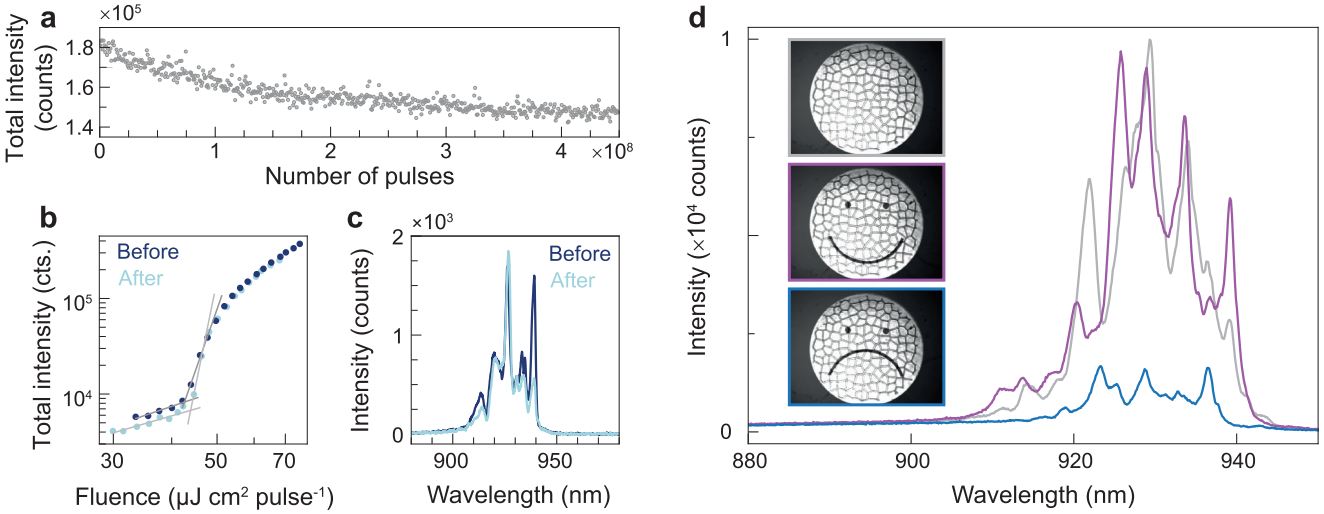

Figure 4. Emission stability and spectral sensitivity of InP network lasers. a) The emission intensity of a network with 150 μm diameter, 7 μm average link length, and 550 nm waveguide width stays stable over many excitation pulses. The total emission intensity decreases by 20% over 4.5 × 10^8 excitation pulses. The device was pumped above threshold with 633 nm, 200-fs pulsed, 100 kHz laser and a spectrum was acquired every 5 s. b) Light-light curves indicating the threshold of the network before (dark blue) and after (light blue) the stability test. c) Emission spectra of first (dark blue) and last (light blue) measurement of the stability test in (a). d) Pumping the network with different spatial patterns: full circle (grey), happy face (purple), and sad face (blue) strongly affects the emission spectra.

3. Discussion

Semiconductor networks provide a novel cavity framework for microlasers, with the flexibility to control the coupling, spatial and spectral distribution of the photonic modes, by proper design of the network topology and the individual links. If the density of the network is too sparse and the length of the links is larger than the gain length, then individual links may lase independently. Instead, collective lasing from network modes delocalized over many links can occur for optimal network design that favors forward transmission into adjoining links and reduces scattering at nodes. This requires waveguides to support efficient transmission and high modal gain for TE01 mode in the network. Efficient network lasers are obtained for networks with node and edge densities optimized to sculpt modes with optimal spatial localization. This optimal design is the result of low overlap with the lossy network edges, and minimal out-of plane losses at the network nodes.

Controlling the spatial overlap and mode extent is important for designing the non-linear response of the lasers to pump input, for applications involving sensing, cryptography and machine learning. The network laser sensitivity is especially important for machine learning applications where the pump profile could be used as an input layer for an optical neuromorphic device. Integration of input-sensitive network lasers on-chip with both passive and active components for out-coupling light and locally controlling the phase of light on links is an exciting prospect. As a first step, network lasers with III-V semiconductor quantum wells could be developed to reduce linewidth broadening and blue shift of the gain with pump power and to tune the emission wavelength to the transparency window for Si photonics. Future work may also investigate reducing the footprint and threshold of network lasers further, for example by optimizing the shape of the nodes or investigating other network topologies. Lasing with lower peak power and ns optical pulses will enable more compact and practical integrated systems to be realized.

To conclude, we demonstrate the first semiconductor, on-chip network random lasers, made of InP bonded on SiO_2/Si substrate. These networks exhibit low threshold of operation, as low as 60 μJcm^{-2} $pulse^{-1}$, multimode emission and sensitivity to the spatial illumination. They are also resilient toward degradation. We design network lasers with optimal properties to minimize the lasing threshold. For specific applications, we show that one needs to consider the design of individual components as well as the overall layout. We show that the total energy at threshold versus pump fraction can be used to probe the spatial distribution of the lasing modes. Semiconductor network lasers are versatile, designable, and easily integrated on-chip. InP is widely used in industry for manufacturing active devices for integrated photonic circuits. Our InP network lasers are fabricated using mainstream processes and so the high cost and complexity of fabrication can be mitigated by scaling up in a commercial foundry. Therefore, we see potential for network lasers, integrated with passive photonic waveguides, to serve as a multifrequency light source that is controlled by the excitation. A particularly promising application is for physical machine learning due to possible control of the lasing output through pump pattern variations. In addition, on-chip semiconductor networks are attractive for use in signal processing, optical communication and hardware security.

4. Experimental Section

Network Design: Networks were designed by using a random point pattern on a plane and generating a Voronoi diagram. The networks were cropped to circular areas with diameters ranging between 30 and 150 µm, and the density of the point patterns was varied to generate networks with average link lengths ranging between 2 and 10 µm.

Fabrication: The samples were fabricated using a Direct Wafer Bonding approach. A layer of InP was grown on a sacrificial III-V semiconductor wafer, assuring lattice constant matching and defect-free growth. The III-V wafer was bonded via annealing to a Si wafer with 2 µm-thick SiO_2 layer to provide optical isolation from the substrate. The sacrificial wafer was then removed by wet etching, leaving the InP active layer bonded to the Si wafer, which was subsequently cleaved into chips. Hydrogen Silsesquioxane (HSQ) was then deposited on a chip by spin-coating and patterned into a hard mask with electron beam lithography. Finally, Inductively Coupled Plasma Reactive Ion Etching (ICP-RIE) was used to transfer the mask pattern onto the InP layer. The chips were treated with phosphoric acid to clean and passivate the InP walls post-etch, and then coated with a few nanometers of Al_2O_3 using Atomic Layer Deposition (ALD) to complete the passivation and stop further oxide formation on the surfaces.[42]

Lasing Experiments: The InP networks were characterized in a micro photoluminescence setup. They were pumped with a 633 or 700 nm, 200 fs-pulsed laser at 100 kHz. The pump beam was focused on the sample from the top through a 20x objective. The emitted light was also collected from the top through the same objective and measured in a Princeton Instruments spectrometer (spectral resolution 0.25 nm, integration time 1 s). The pump beam was reflected off a digital micromirror device (DMD), which consists of 1280 × 800 programmable mirror pixels, and could be shaped into a top-hat beam with a defined diameter. The exact power at the sample was measured for every spectrum by inserting a glass slide in the beam path before the objective that reflects part of the beam into a calibrated powermeter.

FDTD Simulations: Finite-difference time-domain (FDTD) simulations in Ansys Lumerical were used to evaluate the transmission of guided modes. Guided modes within the links were evaluated numerically using an eigenmode solver and scattering loss at the network nodes was simulated by injecting a mode along a link and measuring the fraction of power that is guided within the same mode or into different modes in each connecting link. The waveguide geometry was similar to the fabricated structures, with HSQ/InP waveguide (thickness 110 and 120 nm, respectively) lying on top of a SiO_2 substrate. A refractive index of 1.5 was specified for both SiO_2 and HSQ and 3.4 for InP, and modes were evaluated at a free-space wavelength of 900 nm. Simulations were performed for a Y-branch with a 120° angle between each link and for different link cross-section dimensions.

netSALT modeling: Network laser modes and threshold were modeled using netSALT,[24] where the network is represented as a graph, with a complex refractive index specified on each edge ($n = 3.4 + 0.01i$). The pump was defined on certain edges within a specified circular region and the trajectories of the modes in the complex k plane, where k is the wavenumber, were tracked as the pump power was increased. The pump power of the first mode to reach threshold, defined as when the imaginary part of the mode wavenumber reaches zero, was used for modeling the threshold versus pump size dependence.

Supporting Information

Supporting Information is available from the Wiley Online Library or from the author.

Acknowledgements

The samples were fabricated in the Binnig and Rohrer Nanotechnology Center (BRNC) at IBM Research Europe - Zurich. The authors thank Markus Scherrer, Daniele Caimi, and the Cleanroom Operations Team of

the BRNC for their help and support. The authors also thank Stefano Vezzoli for assistance with the optical setup.

This work was financially supported by the European Union Horizon 2020 Marie Skłodowska-Curie Individual Fellowship grant 800410 (D.S.), the European Union Innovative Training Networks European Industrial Doctorates grant 859841 (A.F., J.D., H.S., and K.M.), the Imperial College President's PhD Scholarship (W.K.N.), the Engineering and Physical Sciences Research Council grant EP/T027258 (D.S., T.V.R., M.B., O.H., and R.S.), and the Science Foundation Ireland (SFI) grant 18/RP/6236 (O.H.)

Conflict of Interest

The authors declare no conflict of interest.

Author Contributions

D.S. and A.F. contributed equally to this work. D.S., A.F., K.M., and R.S. conceptualized the study; D.S., A.F., J.D., N.V.T., T.V.R., and A.A. were associated with methodology; D.S., A.F., J.D., W.K.N., and T.V.R. performed investigations; D.S., A.F., and J.D. contributed to visualization; H.S., M.B., O.H., K.M., and R.S. supervised the study; D.S., A.F., and R.S. wrote the original draft; All authors reviewed and edited the final manuscript.

Data Availability Statement

The data that support the findings of this study are available from the corresponding author upon reasonable request.

Keywords

III-V semiconductor network, InP photonic network, network laser, random laser

Received: May 1, 2024
Revised: July 25, 2024
Published online:

[1] Z. Wang, A. Abbasi, U. Dave, A. De Groote, S. Kumari, B. Kunert, C. Merckling, M. Pantouvaki, Y. Shi, B. Tian, K. Van Gasse, J. Verbist, R. Wang, W. Xie, J. Zhang, Y. Zhu, J. Bauwelinck, X. Yin, Z. Hens, J. Van Campenhout, B. Kuyken, R. Baets, G. Morthier, D. Van Thourhout, G. Roelkens, *Laser Photonics Rev.* **2017**, *11*, 1700063.
[2] N. Li, G. Chen, D. K. T. Ng, L. W. Lim, J. Xue, C. P. Ho, Y. H. Fu, L. Y. T. Lee, *Adv. Opt. Mater.* **2022**, *10*, 2201008.
[3] Z. Zhou, X. Ou, Y. Fang, E. Alkhazraji, R. Xu, Y. Wan, J. E. Bowers, *eLight* **2023**, *3*, 1.
[4] J. Feldmann, N. Youngblood, M. Karpov, H. Gehring, X. Li, M. Stappers, M. Le Gallo, X. Fu, A. Lukashchuk, A. S. Raja, J. Liu, C. D. Wright, A. Sebastian, T. J. Kippenberg, W. H. P. Pernice, H. Bhaskaran, *Nature* **2021**, *589*, 52.
[5] A. Skalli, J. Robertson, D. Owen-Newns, M. Hejda, X. Porte, S. Reitzenstein, A. Hurtado, D. Brunner, *Opt. Mater. Express* **2022**, *12*, 2395.
[6] H. Cao, R. Chriki, S. Bittner, A. A. Friesem, N. Davidson, *Nat. Rev. Phys.* **2019**, *1*, 156.
[7] C. Tu, M. Fränzl, Q. Gao, H. Tan, C. Jagadish, H. Schmitzer, H. P. Wagner, *Adv. Opt. Mater.* **2020**, *9*, 3.
[8] M. Yoshida, S. Katsuno, T. Inoue, J. Gelleta, K. Izumi, M. De Zoysa, K. Ishizaki, S. Noda, *Nature* **2023**, *618*, 727.
[9] R. Lin, V. Mazzone, N. Alfaraj, J. Liu, X. Li, A. Fratalocchi, *Laser Photonics Rev.* **2020**, *14*, 2.
[10] L. Yang, G. Li, X. Gao, L. Lu, *Nat. Photonics* **2022**, *16*, 279.
[11] M. Scherrer, C.-W. Lee, H. Schmid, K. E. Moselund, *ACS Photonics* **2024**.
[12] X. Qiao, B. Midya, Z. Gao, Z. Zhang, H. Zhao, T. Wu, J. Yim, R. Agarwal, N. M. Litchinitser, L. Feng, *Science* **2021**, *372*, 403.
[13] M. Trivedi, D. Saxena, W. K. Ng, R. Sapienza, G. Volpe, *Nat. Phys.* **2022**, *18*, 939.
[14] M. Rashidi, H. H. Tan, S. Mokkapati, *Optica* **2021**, *8*, 1160.
[15] J. Liu, P. D. Garcia, S. Ek, N. Gregersen, T. Suhr, M. Schubert, J. Mørk, S. Stobbe, P. Lodahl, *Nat. Nanotechnol.* **2014**, *9*, 285.
[16] M. Lee, S. Callard, C. Seassal, H. Jeon, *Nat. Photonics* **2019**, *13*, 445.
[17] B. Kumar, R. Homri, P. Sebbah, *Sci. Rep.* **2023**, *13*, 1.
[18] A. S. Gomes, A. L. Moura, C. B. de Araújo, E. P. Raposo, *Progr. Quant. Electr.* **2021**, *78*, 100343.
[19] R. Sapienza, *Nat. Phys.* **2022**, *18*, 976.
[20] H. Noh, J.-K. Yang, S. F. Liew, M. J. Rooks, G. S. Solomon, H. Cao, *Opt. Lett.* **2011**, *36*, 3560.
[21] R. Dhanker, A. N. Brigeman, A. V. Larsen, R. J. Stewart, J. B. Asbury, N. C. Giebink, *Appl. Phys. Lett.* **2014**, *105*, 15.
[22] S. Lepri, C. Trono, G. Giacomelli, *Phys. Rev. Lett.* **2017**, *118*, 123901.
[23] M. Gaio, D. Saxena, J. Bertolotti, D. Pisignano, A. Camposeo, R. Sapienza, *Nat. Commun.* **2019**, *10*, 226.
[24] D. Saxena, A. Arnaudon, O. Cipolato, M. Gaio, A. Quentel, S. Yaliraki, D. Pisignano, A. Camposeo, M. Barahona, R. Sapienza, *Nat. Commun.* **2022**, *13*, 6493.
[25] L. M. Massaro, S. Gentilini, A. Portone, A. Camposeo, D. Pisignano, C. Conti, N. Ghofraniha, *ACS Photonics* **2021**, *8*, 376.
[26] C. Gong, Z. Qiao, S. Zhu, W. Wang, Y.-C. Chen, *ACS Nano* **2021**, *15*, 15007.
[27] N. Caselli, A. Consoli, A. M. Mateos Sánchez, C. López, *Optica* **2021**, *8*, 193.
[28] H. Zhu, W. Zhang, J. Zhang, R. Ma, Z. Wang, Y. Rao, X. Li, *Adv. Mater. Technol.* **2021**, *6*, 9.
[29] J. Dranczewski, A. Fischer, P. Tiwari, M. Scherrer, D. Saxena, H. Schmid, R. Sapienza, K. Moselund, *Micro Nano Eng.* **2023**, *19*, 100196.
[30] B. R. Bennett, R. A. Soref, J. A. Del Alamo, *IEEE J. Quantum Electron.* **1990**, *26*, 113.
[31] J. Tatebayashi, S. Kako, J. Ho, Y. Ota, S. Iwamoto, Y. Arakawa, *Nat. Photonics* **2015**, *9*, 501.
[32] P. Tiwari, P. Wen, D. Caimi, S. Mauthe, N. V. Trivi no, M. Sousa, K. E. Moselund, *Opt. Express* **2021**, *29*, 3915.
[33] A. Fischer, T. V. Raziman, W. K. Ng, J. Clarysse, D. Saxena, J. Dranczewski, S. Vezzoli, H. Schmid, K. Moselund, R. Sapienza, *npj Nanophoton.* **2024**, *1*, 1.
[34] S. Mauthe, N. Vico Trivi no, Y. Baumgartner, M. Sousa, D. Caimi, T. Stöferle, H. Schmid, K. E. Moselund, *IEEE J. Sel. Top. Quantum Electron.* **2019**, *25*, 1.
[35] Y. Ling, H. Cao, A. L. Burin, M. A. Ratner, X. Liu, R. P. H. Chang, *Phys. Rev. A* **2001**, *64*, 6.
[36] M. Bahoura, K. Morris, G. Zhu, M. Noginov, *IEEE J. Quantum Electron.* **2005**, *41*, 677.
[37] L. A. Coldren, S. W. Corzine, M. Mashanovitch, *Diode Lasers and Photonic Integrated Circuits*, 2nd ed., Wiley, Hoboken, NJ **2012**.
[38] T. J. Sturges, M. D. Anderson, A. Buraczewski, M. Navadeh-Toupchi, A. F. Adiyatullin, F. Jabeen, D. Y. Oberli, M. T. Portella-Oberli, M. Stobińska, *Sci. Rep.* **2019**, *9*, 19396.
[39] J. T. Robinson, K. Preston, O. Painter, M. Lipson, *Opt. Express* **2008**, *16*, 16659.
[40] D. Dai, *Proc. IEEE* **2018**, *106*, 2117.
[41] C. Z. Ning, *Phys. Status Solidi (b)* **2010**, *247*, 774.
[42] M. L. Huang, Y. C. Chang, C. H. Chang, Y. J. Lee, P. Chang, J. Kwo, T. B. Wu, M. Hong, *Appl. Phys. Lett.* **2005**, *87*, 252104.